

# On the interface polaron formation in organic field-effect transistors

G. De Filippis<sup>1</sup>, V. Cataudella<sup>1</sup>, S. Fratini<sup>2</sup> and S. Ciuchi<sup>3</sup>

<sup>1</sup>*CNR-SPIN and Dip. di Scienze Fisiche - Università di Napoli Federico II - I-80126 Napoli, Italy*

<sup>2</sup>*Institut Néel - CNRS and Université Joseph Fourier BP 166, F-38042 Grenoble Cedex 9, France*

<sup>3</sup>*CNR-ISC, CNISM and Dipartimento di Fisica, Università dell'Aquila, via Vetoio, I-67010 Coppito-L'Aquila, Italy*

A model describing the low density carrier state in an organic single crystal FET with high- $\kappa$  gate dielectrics is studied. The interplay between charge carrier coupling with inter-molecular vibrations in the bulk of the organic material and the long-range interaction induced at the interface with a polar dielectric is investigated. This interplay is responsible for the stabilization of a polaronic state with an internal structure extending on few lattice sites, at much lower coupling strengths than expected from the polar interaction alone. This effect could give rise to polaron self-trapping in high- $\kappa$  organic FET's without invoking unphysically large values of the carrier interface interaction.

## I. INTRODUCTION

Organic field-effect transistors (OFETs) are the elementary building blocks of “plastic electronics”.<sup>1</sup> In these devices, charges are induced in a thin conducting channel at the interface between an organic semiconductor and a gate insulator. While commercial applications have already appeared, mostly based on low-cost organic thin-films, the fundamental physical mechanisms governing the charge dynamics in these devices are not fully understood. As it has become clear in recent years, even when high purity crystalline semiconductors are used in order to minimize the effects of structural and chemical disorder, the electronic characteristics of OFETs are strongly affected by interactions taking place both within the semiconducting material as well as with its close environment. This can be traced back to the extremely narrow electronic bands resulting from the weak van der Waals intermolecular bonding, that make organic semiconductors much more sensitive to electronic interactions than their inorganic counterparts. For this reason, polaronic effects have been shown to play an important role in these devices.

Several electron-lattice interaction mechanisms relevant to organic molecular crystals have been identified and studied in the past. These include Holstein-like couplings to intra-molecular vibrations, leading to a local reorganization of the molecular energy levels<sup>2–6</sup> as well as Su-Schrieffer-Heeger (SSH) or Peierls-like couplings where the transfer integrals between the molecules are modulated by the inter-molecular motion.<sup>6–10</sup> The latter mechanism couples directly the electronic motion to the strong lattice fluctuations arising from the mechanical softness of these compounds, and has been recently identified as the dominant limiting factor of the charge mobility in pure crystalline semiconductors.<sup>10–14</sup>

In addition to such intrinsic mechanisms, interface-related effects have also been demonstrated in several systematic studies of organic FETs using different gate dielectrics. Sources of charge trapping have been identified, either related to the interface quality<sup>15,16</sup> or to the long-range forces arising from polar impurities at the organic/dielectric interface.<sup>17–20</sup> Furthermore, it has been

shown that the long-range polarization induced in high- $\kappa$  gate materials by the charge carriers themselves can lead to self-trapping of the carriers. Even when sufficient care is taken in order to minimize extrinsic sources of disorder, Fröhlich polarons are formed due to the polar long-range interaction of the carriers in the organic semiconductor with the phonons at the semiconductor/dielectric interface. The strength of this remote electron-phonon (e-ph) interaction can be tuned by an appropriate choice of the gate dielectric. The “metallic-like” carrier mobility characteristic of crystalline organic semiconductors can be converted into a much lower, thermally activated mobility.<sup>21–23</sup>

While there is a vast theoretical literature dedicated to the different electron-lattice interaction mechanisms mentioned above, up to now there have been no attempts to study the interplay between bulk and interface e-ph couplings. To fill this gap, in this work we analyze a model that includes both bulk and interface effects as can be realized in organic FETs, and treat them in a common framework. We focus on the combined effects of the SSH coupling of the electronic transfer integrals to the inter-molecular vibrations and of a Fröhlich long-range e-ph interaction as induced by the presence of the gate dielectric in a field-effect geometry. Apart from its relevance to organic/dielectric interfaces, from the fundamental viewpoint this model presents an interesting combination of two *a priori* competitive mechanisms. Our results show that a rather weak SSH coupling strength as estimated in Refs.[10,11] can have an unexpectedly strong effect in stabilizing a polaronic state when a moderate long-range polar coupling is present. Therefore, self-trapped states of small radius can exist at common organic/dielectric interfaces, even in such cases where the carrier-interface phonon interaction alone would not be sufficient to produce polaronic self-localization<sup>19</sup>. This provides a microscopic theoretical basis for the experimental results of Ref. 21, where a finite activation energy indicative of self-trapped states was observed using gate materials such as Al<sub>2</sub>O<sub>3</sub> and Ta<sub>2</sub>O<sub>5</sub>.

This paper is organized as follows. The model under study is introduced in Section II. The two methods of solution that will be used are described in Section III. In

Section IV we introduce the main quantities of interest and present the results of our calculations. Section V is devoted to the conclusions. A detailed derivation of the form of the long-range interaction with the gate material is presented in Appendix A.

## II. THE MODEL

We consider the following one dimensional tight-binding model

$$\begin{aligned} H = & -t \sum_i [1 + \alpha(a_i + a_i^\dagger - a_{i+1} - a_{i+1}^\dagger)] (c_i^\dagger c_{i+1} + H.c.) \\ & + \sum_{i,q} c_i^\dagger c_i (M_q e^{iqR_i} b_q + h.c.) \\ & + \omega_{SSH} \sum_i a_i^\dagger a_i + \omega_{LR} \sum_q b_q^\dagger b_q \end{aligned} \quad (1)$$

where electrons or holes described by the creation and destruction operators  $c_i^\dagger, c_i$  move on a lattice labelled by site index  $i$ . These interact with molecular displacements  $X_i = a_i^\dagger + a_i$  via a SSH interaction, describing the transfer integral modulation on the distance between nearest neighbors with strength  $\alpha$ , as well as with optical modes  $Y_q = b_q + b_{-q}^\dagger$  at the polar interface via a coupling  $M_q$ . To keep the discussion as simple as possible and illustrate the main consequences of the interplay between the “off-diagonal” short range SSH coupling and the “diagonal” long-range polar coupling, we shall restrict the electronic motion to a one-dimensional chain. Yet, our results can be considered as being qualitatively representative of organic/dielectric interfaces in the more realistic two-dimensional case.

As it is discussed in Appendix A we consider the one dimensional interface model introduced in Refs.[24,25]. The e-ph interaction matrix element reads in this case

$$M_q = \frac{g}{\sqrt{N}} \sum_i e^{iqR_i} \frac{R_0^2}{R_0^2 + R_i^2} \quad (2)$$

with  $R_0$  a cut-off length of the order of the lattice spacing  $a$  and  $q$  a strictly one-dimensional vector. As it is clear from Eq. (2), the interaction between the electron charge and the associated lattice polarization is long ranged, with a power law decay in real space. We define two dimensionless coupling constants for the two different el-ph couplings:

$$\lambda_{LR} = \sum_q \frac{|M_q|^2}{2\omega_{LR}t} \quad (3)$$

and

$$\lambda_{SSH} = \frac{\alpha^2 t}{\omega_{SSH}}. \quad (4)$$

We shall study the system in the range of parameters typical of single crystal organic semiconductors, taking

rubrene as a case study. We set  $\omega_{LR} = 0.25t$  as an average value for the interface phonons in the case of common polarizable gate materials<sup>21</sup> and  $\omega_{SSH} = 0.05t$  for the relevant intermolecular vibrations<sup>11,14</sup> ( $\hbar = 1$  throughout the paper). The lattice cutoff parameter entering in Eq. (2) is chosen to be  $R_0 = 0.5a$ .<sup>26</sup>

In view of the small values of  $\omega_{LR}$  and  $\omega_{SSH}$ , we will study the system by using two approaches: the adiabatic approximation, valid for vanishing  $\omega_{LR}$  and  $\omega_{SSH}$ , and a variational exact diagonalization (VED) method able to include non adiabatic contributions.

## III. METHODS

### A. Adiabatic approximation

For values of  $\omega_{LR}$  and  $\omega_{SSH}$  that are much smaller than  $t$ , the lattice polarization cannot follow the electronic oscillations and the wave function of the system can be factorized<sup>27</sup> into a product of normalized variational functions  $|\varphi\rangle$  and  $|f\rangle$  depending on the electron and phonon coordinates respectively:

$$|\psi\rangle = |\varphi\rangle |f\rangle \quad (5)$$

where

$$|\varphi\rangle = \sum_{R_m} c_m^\dagger |0\rangle_{el} \phi(R_m) \quad (6)$$

This factorization becomes exact when we neglect completely the ionic kinetic energy i.e.  $\omega_{SSH}, \omega_{LR} \rightarrow 0$ . In Eq.(6),  $|0\rangle_{el}$  is the electron vacuum state and  $\phi(R_m)$  are parameters that satisfy the relation:

$$\sum_m |\phi(R_m)|^2 = 1. \quad (7)$$

The expectation value of the Hamiltonian (1) on the state  $|\varphi\rangle$  provides an effective Hamiltonian for the lattice fields:

$$\begin{aligned} \langle \varphi | H | \varphi \rangle = & -t \sum_m [\phi^*(R_m) \phi(R_m + 1) + h.c.] \\ & + \sum_q [\omega_{LR} b_q^\dagger b_q + (\rho_q b_q + H.c.)] \\ & + \sum_m [\omega_{SSH} a_m^\dagger a_m + (v_m a_m + H.c.)] \end{aligned} \quad (8)$$

with

$$\rho_q = M_q \sum_i e^{iqR_i} |\phi(R_i)|^2 \quad (9)$$

and

$$v_m = -\alpha t [(\phi(R_{m+1}) - \phi(R_{m-1})) \phi^*(R_m) + h.c.]. \quad (10)$$

It can be proven that the ground state of this Hamiltonian is a product of two coherent states:

$$|f\rangle = e^{\sum_q \left( \frac{\rho_q}{\omega_{LR}} b_q - h.c. \right)} |0\rangle_{LR} e^{\sum_m \left( \frac{v_m}{\omega_{SSH}} a_m - h.c. \right)} |0\rangle_{SSH}, \quad (11)$$

where  $|0\rangle_{LR}$  and  $|0\rangle_{SSH}$  are the vacuum states of the two lattice fields. We stress that the parameters  $v_m$  are real [see Eq.(10)].

At this stage, the phonon state  $|f\rangle$  can be used to obtain an effective Hamiltonian for the charge carrier:

$$H_{eff} = -t \sum_i [1 + 2\alpha(v_i - v_{i+1})] (c_i^\dagger c_{i+1} + c_{i+1}^\dagger c_i) - \sum_i c_i^\dagger c_i \sum_q (M_q e^{iqR_i} \rho_q^* + h.c.) + K \quad (12)$$

where

$$K = \omega_{LR} \sum_q |\rho_q|^2 + \omega_{SSH} \sum_m v_m^2. \quad (13)$$

The present adiabatic approximation breaks translational invariance. The problem is reduced to studying an electron, confined by the potential well raised by the LR interaction. The hopping amplitude from site to site within the well depends on the specific site pair, via the SSH coupling. The wavefunction parameters  $\phi(R_m)$  are determined variationally.

## B. The VED diagonalization technique

In the systems on which we are focusing our attention the phonon frequencies  $\omega_{SSH}$  and  $\omega_{LR}$  are small compared to the transfer integrals.<sup>11</sup> The adiabatic approach discussed above should therefore provide a reasonably appropriate description of the ground state properties. It is known, however, that a proper inclusion of non adiabatic terms in the calculation removes the fictitious translational symmetry breaking, which is found within the pure adiabatic approximation, and can introduce significative changes at any non-zero phonon frequencies. Furthermore physical quantities related to the quantum nature of the phonons (number of phonons in the ground state) or the delocalization of the electronic wave function (effective mass and ground state spectral weight) can be accessed only via a non adiabatic approach. To this aim we implement here a method, combining a variational approach and an exact diagonalization technique, which is able to provide an accurate description of the ground state properties at all values of the system parameters. We shall first analyze the two interactions separately, and then introduce the method for treating the full Hamiltonian Eq. (1).

It has been shown<sup>28-31</sup> that the ground state features in the case of “diagonal” electron-lattice interactions, such as the LR term Eq. (2), are very well reproduced by methods assuming as starting point the approach introduced by Toyozawa.<sup>32</sup> The idea is to restore a translationally invariant Bloch state using the wavefunctions

provided by the adiabatic approximation, i.e. by taking a superposition of localized states centered on different lattice sites. The trial wave function that accounts for the translational symmetry reads:

$$|\psi_k^{(LR)}\rangle = \frac{1}{\sqrt{N}} \sum_n e^{ikR_n} |\psi_k^{(LR)}(R_n)\rangle \quad (14)$$

where

$$|\psi_k^{(LR)}(R_n)\rangle = \sum_l c_{l+n}^\dagger |0\rangle_{el} \phi_k(R_l) |e_n^{(LR)}\rangle \quad (15)$$

and

$$|e_n^{(LR)}\rangle = e^{\sum_q \left( e^{iqR_n} \frac{\rho_q}{\omega_{LR}} b_q - h.c. \right)} |0\rangle_{LR}. \quad (16)$$

In Eqs.(14-16) the index  $n$  denotes the distance between the electron position and the lattice modes.

The next step is to generalize this wavefunction to correctly recover the weak coupling regime where the electron is weakly dressed by lattice oscillations, as predicted by perturbation theory. This can be achieved by treating the parameters entering into the definition of the function  $\rho_q$  as independent variational parameters,<sup>30</sup> rather than being constrained by the shape of the electron function as in Eq. (9). Actually, also in the perturbative regime the lattice displacement is described by a coherent state, but with a different function  $\rho_q$  including an electron recoil term due to the scattering with phonons.<sup>28,29</sup> The parameters  $\phi_k(R_l)$  have to be determined via numerical diagonalization of the corresponding Hamiltonian, defining the Variational Exact Diagonalization method described below. In this way we obtain a wavefunction that is able to capture the weak and strong coupling limits and interpolates between them in the intermediate regime.

In practice we use a basis where each vector is a linear superposition, with appropriate phase factors, of the translational copies of a state having a given electron position and lattice configurations (phonons and electron are translated together, with their relative position being held fixed). We choose as phonon states those appearing in Eq. (16) where  $\rho_q$  is a variational function. There are then  $M$  basis vectors, labelled by the  $n$  index appearing in Eq. (16), and each of them includes the variational function  $\rho_q$ . The coefficients  $\phi_k(R_l)$  in Eq.(15) are determined for each fixed set of the parameters defining the variational function  $\rho_q$  by diagonalizing the Hamiltonian matrix in the chosen basis. These do not coincide, in general, with the coefficients of the function  $\rho_q$  in Eq.(9). Summarizing, we have to diagonalize a  $M \times M$  matrix for each value of the variational function  $\rho_q$ . Finally, in the following, we assume that the variational parameters  $\phi(R_l)$ , entering into the definition of the function  $\rho_q$  in Eq. (9), are different from zero up to 3rd nearest neighbors. We have checked that this assumption allows to obtain convergency for all the values investigated of the model parameters.

The procedure described above could be straightforwardly generalized to include also the interaction with

SSH phonons. Unfortunately, it can be shown that it does not capture the correct physical features of the SSH Hamiltonian in the absence of LR interaction.<sup>33</sup> To treat the SSH term we therefore apply a different approach based on an exact diagonalization procedure, where we do not assume as basis set the coherent states of the adiabatic approach. In this approach the phonon variables are efficiently limited to a new set which is able to describe successfully the ground state properties, as it will be shown below. The real bottleneck comes from the phonon Hilbert space, that is infinite. To circumvent this difficulty, we keep states where the lattice deformations involve only the sites up to 3rd nearest neighbors of the lattice site where electron is located, all the others being undeformed

$$|ph\rangle(n_j, j = -3, \dots, 3) = \prod_{j, i \neq j}^{j=-3, \dots, 3} \frac{(a_{n+j}^\dagger)^{n_j} |0\rangle_{n+j} |0\rangle_i}{\sqrt{n_j!}} \quad (17)$$

where  $n$  indicates the electron position. We apply a truncation procedure considering only the states with at most  $L$  quanta, i.e.  $\sum_j n_j \leq L$ , where  $L$  is fixed by requiring convergence of the ground state energy. These states provide a correct physical description of the ground state properties, since the lattice deformations are effectively localized around the site where the electron is located. Furthermore, in analogy with the LR coupling, we use the translational symmetry associated to periodic boundary conditions to reduce the size of the sparse Hamiltonian matrix, requiring that the states have a definite momentum.

When both LR and SSH couplings are considered, we adopt a VED diagonalization technique on a truncated phonon basis that combines the two subspaces introduced separately for the  $\alpha = 0$  and  $g = 0$  cases. This basis is given by the product of the vectors describing the two different couplings separately, Eqs. (16) and (17). The ground state is found by using the modified Lanczos algorithm.<sup>34</sup> We emphasize that this approach retains the full translational invariance requiring that each basis vector has a well defined momentum.

#### IV. RESULTS

Due to their different microscopic nature, the two interaction terms in Eq. (1) induce different types of polaron states: the LR coupling to the electron density favors localized states centered on the lattice sites (site polaron), while the SSH coupling to the electronic transfer integrals tends to localize the polarons on inter-molecular bonds, i.e. with the electronic charge centered between two neighboring molecular sites (bond polaron). This competition results in the phase diagrams reported in Fig. 1, which constitute the central results of this paper. The most notable feature is the existence of a reentrant phase where a bond polaron state is stabilized by the interplay between the two microscopic interaction mechanisms.

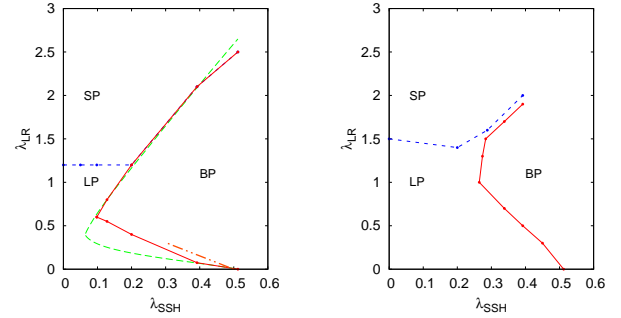


FIG. 1: Phase diagram a) in the adiabatic approximation and b) in the VED approximation. The dashed (blue) line marks the crossover from large (LP) to small (SP) site-centered polaron probed by the bimodality of the LR-PDF. The solid (red) line indicates the crossover to the bond polaron (BP) state probed by the bimodality of the SSH-PDF while the dashed (green) line is the transition to the bond polaron state probed by the electronic wavefunction (only in panel a). In panel a) the dashed double dotted red line is the analytic estimate of Eq. (20).

This result is robust against the presence of phonon quantum fluctuations, as is apparent from the comparison of the phase diagram obtained from the adiabatic approximation, valid in the limit of vanishing frequencies  $\omega_{SSH}, \omega_{LR} \rightarrow 0$  [Fig.1 (a)], with the results at finite phonon frequencies [Fig.1 (b)].

##### A. Adiabatic approximation

In the adiabatic approximation the ground state electronic wave function is always localized. However, for small values of  $\lambda_{SSH}$ , a crossover from a large to a small site-centered polaron occurs upon increasing the LR interaction strength  $\lambda_{LR}$  [blue dashed line in Fig. 1 (a)]: the wavefunction extension is progressively reduced, being always centered on a given molecular site. The locus of the crossover can be determined by analyzing the qualitative changes induced on the phonon wavefunction, as described at the end of this Section. The large to small polaron crossover is only weakly affected by the presence of the SSH interaction.

As  $\lambda_{SSH}$  increases, the symmetry of the electronic wave function changes continuously from site-centered to bond-centered. The breaking of translational invariance allows us to analyze this transition by direct inspection of the electronic wavefunction, which is shown in Fig. 2 together with its associated distortions in the bond-centered (left panel) and site-centered polaron (right panel) states. The transition between the two phases is indicated by the green dashed line in Fig.1a.

Contrary to the large/small polaron crossover, that is rather insensitive to the value of  $\lambda_{SSH}$ , the site to bond-polaron transition is significantly modified by the presence of the LR interaction, which strongly stabilizes the

bond polaron state. The boundary of the bond-centered polaron phase shows a markedly reentrant behavior, reaching a minimum  $\lambda_{SSH} = 0.072$  at  $\lambda_{LR} = 0.4$ .<sup>42</sup>

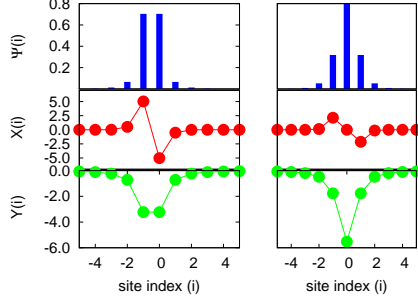


FIG. 2: Bond polaron properties for  $\lambda_{SSH} = 0.4$   $\lambda_{LR} = 1.0$  (left panels) and  $\lambda_{LR} = 1.5$  (right panels) in the adiabatic approximation. Upper panel: the adiabatic electronic probability. Central panel: SSH average distortions of the organic molecular lattice. Lower panel: LR average distortions at the organic/dielectric interface.

It is instructive to understand the stabilization of the bond polaron phase induced by the long-range interface interactions from the following energy balance argument. In the absence of intermolecular coupling ( $\lambda_{SSH} = 0$ ) the energy of the large polaron can be written in general as

$$E_{LP} = -2t - \Delta E_{LP} \quad (18)$$

where the second term can be expanded for small  $\lambda_{LR}$  as  $\Delta E_{LP} = t(a_1\lambda_{LR} + a_2\lambda_{LR}^2 + \dots)$ . On the other hand we see from Fig. 2 that in the bond polaron phase the adiabatic electronic wave function is mainly localized on two neighboring sites, with exponentially vanishing tails on the adjacent molecules. Neglecting such tails provides the following estimate for the bond polaron energy:

$$E_{BP} = -t(1 + 2\lambda_{SSH}) - t(1 + \eta)\lambda_{LR} \quad (19)$$

where the two contributions come respectively from SSH and LR interactions. The parameter  $\eta = \sum_q |M_q|^2 e^{iaq} / \sum_q |M_q|^2$  ( $a$  the lattice spacing,  $0 < \eta < 1$ ) takes into account the spatial variation of the long-range potential-well between two neighboring sites. Comparing the two energies we obtain a transition when

$$\lambda_{SSH} = 1/2 + [a_1 - (1 + \eta)/2]\lambda_{LR}, \quad (20)$$

and a reentrant behavior is found when  $a_1 < (1 + \eta)/2$ . Observing that  $\eta$  is largest for slowly varying potentials, we recognize that the reentrance is strongly favored by the long range nature of the polar dielectric interaction. The reason is that such long-ranged polar interaction, for which the preferred polaronic state would be site-centered, is not extremely sensitive to the local details of the wavefunction, so that it can still provide a sizable energy stabilization in the case of a dimer structure. It

should be stressed that the arguments presented here are only qualitative. For a quantitative analysis of the large polaron to bond polaron phase boundary, the extended nature of the bond polaron wavefunction must be taken into account, which further enhances the reentrant behavior as compared to Eq. (20) (see Fig.1).

Phonon related characteristics also change across the bond polaron transition, following the changes of the electronic wavefunction. As can be seen from Fig. 2, the average SSH distortions within a bond polaron are opposite, since this configuration minimizes the SSH interaction energy. Within the entire bond polaron region of the phase diagram, even at the relatively large value of the LR coupling  $\lambda_{LR} = 1$  illustrated in Fig. 2, the LR distortions follow the charge distribution determined by minimizing the SSH interaction energy.

The phonon probability distribution functions (PDF) provide an alternative tool to characterize the ground state properties,<sup>35</sup> with the advantage of being directly generalizable to the translationally invariant ground states examined in the next section. The SSH-PDF, which represents the distribution of SSH displacements at site  $i + j$  given an electron on site  $i$ , is defined as

$$P_{SSH}^{(j)} = \left\langle |X_{i+j} > c_i^\dagger | 0 > < 0 | c_i < X_{i+j} | \right\rangle \quad (21)$$

where  $|X_{i+j} >$  is the coordinate eigenstate corresponding to the displacement of SSH phonons on site  $i + j$ . The LR-PDF is defined by substituting  $X$  with  $Y$  in Eq. (21). It is worth noting that the PDF is closely related to the distributions of interatomic distances that can be directly measured by neutron spectroscopy such as pulsed neutron diffraction.<sup>36</sup>

The local ( $j = 0$ ) part of these functions is plotted in Fig. 3 for different polaronic ground states. In the small  $\lambda_{SSH}$  region of the phase diagram [see Fig. 1 a)], the large-to-small polaron crossover is highlighted by the bimodality in the LR-PDF [panel (a) of Fig. 3]. On the other hand, when the bond polaron state is *well* formed, the SSH-PDF shows two symmetric peaks [panel (b)], whose distance increases with  $\lambda_{SSH}$ . This provides an alternative method to locate the bond polaron region, which is shown in Fig. 1 (a) as a red continuous line. The resulting phase diagram shows that a broad crossover region emerges (between the green and red lines in Fig. 1 where the electronic wavefunction has already undergone the bond transition but a real bimodality of the SSH-PDF is still not observed, with the SSH-PDF showing large non-Gaussian fluctuations. Let us note that in the bond polaron region of the phase diagram, the analysis of the LR-PDF does not show any evidence of a large to small bond polaron crossover, at least for values of  $\lambda_{SSH} \leq 0.5$ .

Summarizing, the adiabatic phase diagram shows three distinct regimes: small site-centered polaron, large site-centered polaron and bond polaron. The bond polaron regime, with the electron wavefunction mostly localized

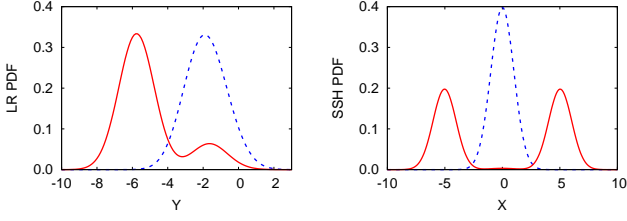


FIG. 3: (left) Local probability distribution function  $P_{LR}^{(0)}(Y)$  of the LR phonons (see text) at  $\lambda_{SSH} = 0$ ,  $\lambda_{LR} = 0.7$  (blue dotted line) and  $\lambda_{LR} = 1.5$  (red solid line); (right) Same for the SSH phonons:  $P_{SSH}^{(0)}(X)$  at  $\lambda_{SSH} = 0.4$ ,  $\lambda_{LR} = 0$  (blue dotted line) and  $\lambda_{LR} = 1$  (red solid line)

on a molecular dimer, is stabilized by the presence of even a moderate long range coupling.

### B. Variational Exact Diagonalization method

Fig. 1 (b) illustrates the phase diagram obtained using the VED scheme described in section III B. Translational symmetry breaking is prevented by the quantum fluctuations of both SSH and LR phonons. Accordingly, all the lines shown in Fig. 1 (b) correspond to *crossover* lines separating translationally invariant states with different characteristics, as obtained by analyzing the phonon PDFs.<sup>35</sup>

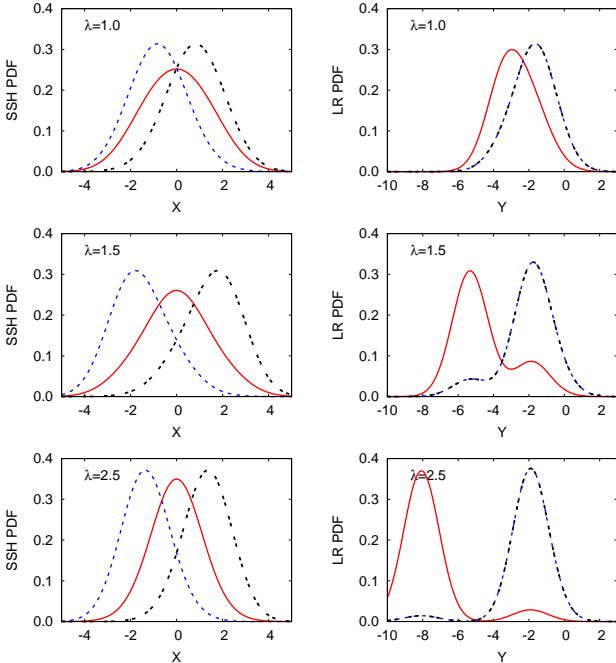


FIG. 4: SSH (left) and LR (right): phonon PDF at  $\lambda_{SSH} = 0.2$ : upper panel:  $\lambda_{LR} = 1.0$ , central panel:  $\lambda_{LR} = 1.5$ , lower panel:  $\lambda_{LR} = 2.5$ . Solid (red) line represents  $j = 0$  (see text); dashed blue (double dashed black) line represents  $j = 1$  ( $j = -1$ ).

In Fig. 4 we plot the SSH-PDF and LR-PDF for  $j = -1, 0, 1$ , in the small  $\lambda_{SSH}$  region (we use  $\lambda_{SSH} = 0.2$ ) of the phase diagram, across the large-to-small polaron crossover [see Fig. 1 (b)]. This crossover is evinced by the bimodality in the LR-PDF, occurring at  $\lambda_{LR} \simeq 1.4$ . Both the on-site ( $j = 0$ ) and the inter-site LR-PDF ( $j = -1, 1$ , which are equal by symmetry), become bimodal at the crossover. In this region, the SSH phonons present a nearly Gaussian distribution with opposite distortions around the polaron localization site. It is interesting to note that the average value of the SSH displacement has a non-monotonic dependence on the LR interaction and it is largest for intermediate values of  $\lambda_{LR}$ , signaling the proximity to the bond polaron regime.

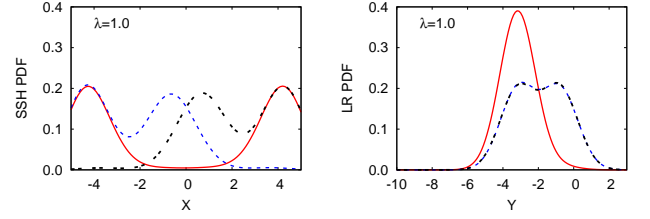


FIG. 5: SSH (left) and LR (right) phonon PDF at  $\lambda_{SSH} = 0.4$  in the bond polaron regime. The solid (red) line represents the on-site contribution,  $j = 0$  (see text); dashed blue (double dashed black) line represents the inter-site part  $j = 1$  ( $j = -1$ ).

In the bond polaron phase both the LR and the SSH-PDF have a bimodal character, as shown in Fig. 5. The SSH-PDF displays bimodality in both the on-site ( $P_{SSH}^{(0)}$ ) and nearest neighbor ( $P_{SSH}^{(\pm 1)}$ ) contributions. The site where the polaron is located belongs to either a left or right-centered dimer, a situation which is consistent with the translational invariance of the ground state. The LR-PDF instead is bimodal only on the nearest neighbor ( $P_{LR}^{(\pm 1)}$ ), with two peaks corresponding to distorted and non-distorted sites respectively. The presence of a distortion with the same amplitude on nearest neighboring sites is another signal of the tendency to form a dimer. This tendency is also displayed by the LR distortions which, in this region of the phase space, follow the charge distribution dictated by the SSH interaction.

Let us note that the reentrant bond polaron phase at  $\lambda_{LR} \neq 0$  has a different symmetry than that at  $\lambda_{LR} = 0$ . Indeed, according to Ref.[37], the transition to the bond polaron phase induces the ground state wavenumber to change continuously from  $k = 0$  to  $k = \pm\pi/2$  in a narrow region around  $\lambda_{SSH} = 0.5$ . As soon as  $\lambda_{LR}$  is different from zero, we do not find any evidence of a  $k \neq 0$  ground state for  $\lambda_{SSH} < 0.5$ . To illustrate this point, the electron dispersion characteristic of this phase, where the minimum is located at  $k = 0$ , is plotted in Fig. 6. We conclude that in the reentrant bond polaron phase, the LR coupling stabilizes a Bloch wavefunction having  $k = 0$ .

In Fig. 7 we plot the inverse effective mass and the



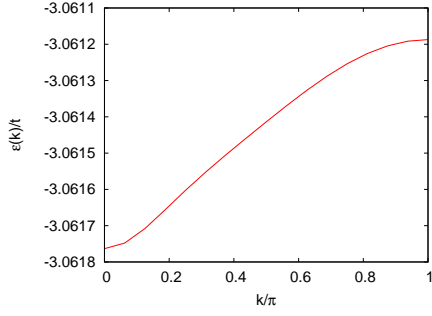


FIG. 6: Polaron band at  $\lambda_{LR} = 1.0$  and  $\lambda_{SSH} = 0.288$  (reentrant bond polaron phase), in units of  $t$ .

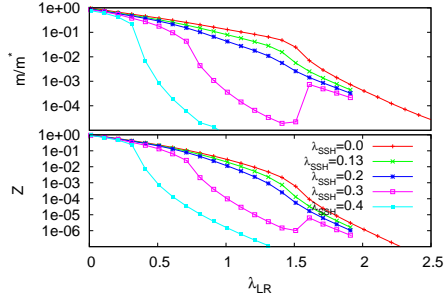


FIG. 7: Inverse effective mass renormalization (upper panel,  $m$  is the band mass) and the quasiparticle spectral weight (lower panel) as a function of  $\lambda_{LR}$  for different values of  $\lambda_{SSH}$ .

quasiparticle weight, defined as  $Z = |\langle GS | c_{k=0}^\dagger | 0 \rangle|^2$ , as a function of  $\lambda_{LR}$  for different values of the SSH coupling  $\lambda_{SSH}$ . At small values of  $\lambda_{SSH}$  the inverse effective mass first decreases smoothly with  $\lambda_{LR}$  and then drops at the large-to-small polaron crossover around  $\lambda_{LR} \simeq 1.4 - 1.5$ . The quasiparticle spectral weight shows a similar dependence on  $\lambda_{LR}$ , although with a steeper reduction which is characteristic of non-local e-ph interactions.<sup>38,39</sup> In contrast with the rather smooth  $\lambda_{LR}$  dependence, a much stronger dependence on  $\lambda_{SSH}$  can be seen in Fig. 7, signaling the crossover into the reentrant bond polaron regime at  $\lambda_{SSH} < 0.5$ . We note that the quasiparticle spectral weight and inverse effective mass have in this case the same behavior with  $\lambda_{LR}$  as it occurs for local e-ph interactions,<sup>39</sup> i.e. they tend to be mutually proportional.

Complementary insight on the electron dynamics in the different phases can be obtained from the analysis of the total kinetic energy,  $E_{kin} = -t \sum_i \langle c_i^\dagger c_{i+1} + c_{i+1}^\dagger c_i \rangle$ , shown in Fig. 8. Unlike the quasiparticle spectral weight  $Z$  and effective mass  $m^*$ , this quantity gets contributions from both the coherent long distance motion of the polaron, and from the internal motion of the electron within the lattice potential-well. The large-to-small polaron crossover at small  $\lambda_{SSH}$  causes a sharp drop of  $E_{kin}$  around  $\lambda_{LR} \simeq 1.5$ . For  $\lambda_{SSH} > 0.25$  a region emerges where the kinetic en-

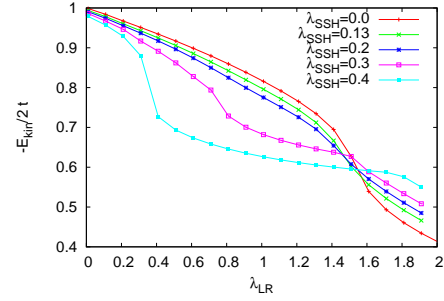


FIG. 8: Electron kinetic energy, in units of the bare kinetic energy ( $\lambda_{SSH} = \lambda_{LR} = 0$ ), as a function of  $\lambda_{LR}$  for different values of  $\lambda_{SSH}$ .

ergy stays relatively constant over a broad range of  $\lambda_{LR}$ . This plateau is another clear signature of the bond polaron phase. Here the effective mass and the quasiparticle spectral weight are very small, indicative of polaron self-trapping, yet a large contribution to the kinetic energy arises from the internal dimer structure of the polaron, with the electron moving freely along the intermolecular localization bond.

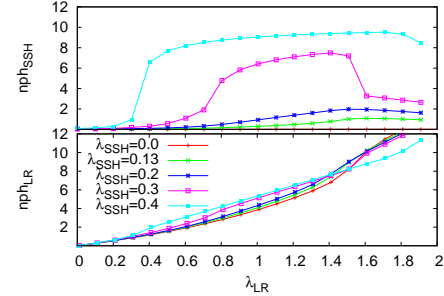


FIG. 9: Average number of SSH (upper panel) and LR phonons (lower panel) in the polaronic ground state as function of  $\lambda_{LR}$  for several values of  $\lambda_{SSH}$ .

The large number of SSH phonons participating in the polaronic state in the reentrant phase, shown in Fig. 9, indicates that a strong coupling with intermolecular modes in the organic crystal can be effectively triggered even at relatively weak values of  $\lambda_{SSH}$ , by suitably turning on the LR interaction. At the same time, the number of LR phonons stays relatively small, exhibiting only a weak dependence on  $\lambda_{SSH}$  (see lower panel of Fig. 9).

## V. CONCLUSIONS

In this paper, we have investigated a microscopic model that describes the interplay between the intermolecular electron-phonon coupling and the additional interaction arising in crystalline organic semiconductors due to the long range polarization at the interface with a gate dielectric, two ingredients that are commonly found

in organic field effect transistors. The ground state properties obtained by two complementary approaches — the adiabatic approximation and a more refined variational method that correctly preserves translational invariance in the presence of phonon quantum fluctuations — demonstrate the synergistic cooperation between bulk and interfacial interactions. In particular, we have found that a large-mass polaronic state with a dimer structure and strong inter-molecular distance fluctuations is stabilized at relatively low values of both the long-range polar coupling  $\lambda_{LR}$  and the intermolecular coupling  $\lambda_{SSH}$ . Such *bond polaron* reentrant phase arises in a region of the phase diagram where the two interactions taken separately would not give rise to strong polaronic effects. The long range nature of the polar interaction is crucial for the establishment of this cooperative interplay. The latter occurs because the long range interface polarization is able to provide a sizable energy gain without much perturbing the local dimer structure dictated by the SSH intermolecular coupling, so that the system can take advantage of both microscopic interaction mechanisms simultaneously.

From the device perspective, our findings provide a microscopic basis to explain the existence of small-radius self-trapped states without invoking unrealistic values of the polar coupling. Indeed, the electrical characteristics of high- $\kappa$  organic FETs have been analyzed in Ref.[21] in terms of the polar interface interaction alone, and the observed thermally activated mobilities are not entirely consistent with the estimated values of  $\lambda_{LR}$ , as has been pointed out in Ref.[19]. The present results show that the proper inclusion of a bulk electron-lattice interaction mechanism such as the intermolecular SSH coupling extends the region of small-radius polaronic self-trapping down to much lower values of  $\lambda_{LR}$ . Let us stress that an analogous interplay as the one studied here can be expected when combining the effects of a bulk intermolecular electron-lattice coupling and the interaction with localized polarizable impurities such as those considered in Refs. [18,19].

Comparing the inter-molecular coupling strength estimated for Rubrene,  $\lambda_{SSH} \simeq 0.17$ ,<sup>11</sup> with the phase diagrams of Fig. 1, we conclude that interfaces involving this organic material and the aforementioned gate materials lie in a region of the phase diagram where the intermolecular/gate synergistic effects are expected to be of relevance. More importantly, our results could explain why at present there are only few organic semiconductors (among which, Rubrene) where metallic-like mobilities have been measured in a FET configuration. Other materials with slightly larger values of the intermolecular coupling strength,  $\lambda_{SSH}$ , would rapidly enter the bond-polaron phase, causing the carriers to undergo a self-trapping transition as soon as a moderate interaction with the dielectric environment is present.

Although the model investigated in this paper includes some drastic approximations, i.e. the model is one-dimensional and the real lattice structure of the organic

FET is not taken into account, we believe that the main conclusions provided here will not be qualitatively modified by the inclusion of more realistic lattice structures and interactions. The detailed study of the transport characteristics in the bond polaron phase identified here remains as an open question for future work.

## Appendix A: Long-range interaction at the interface.

In this work we studied the interplay between SSH and Fröhlich e-ph interactions in one-dimension. While the definition of the SSH coupling in one-dimension is unambiguous,<sup>11</sup> the polar e-ph interaction term depends on the geometry of the interface. We now examine two physically different cases.

The case that is studied in the paper is a truly one-dimensional interface, derived for a wire of square cross-section and permittivity  $\epsilon_1$  embedded in a three-dimensional polar dielectric with permittivity  $\epsilon_2$ .<sup>24,25</sup> We specialize the results of Ref.[25] by allowing the motion of the charges only on the symmetry axis of the interface  $z$  with  $x = 0, y = 0$ , at a distance  $R_0$  from the polar dielectric with permittivity  $\epsilon_2$ . The medium with permittivity  $\epsilon_1$  is taken to be the vacuum. In this geometry the interaction of electrons with the interface phonons reads

$$M_q = M_0 e^{-qR_0} \quad (A1)$$

with  $R_0 = (|x| + |y|)/\sqrt{2}$  or, in real space,

$$f(R) \propto \frac{R_0}{R^2 + R_0^2} \quad (A2)$$

Notice that here the phononic modes are purely one dimensional modes, i.e. they are propagating waves only along the wire (direction  $z$ ).

It is interesting to compare the one dimensional interaction discussed above with a two dimensional model. The model that we consider is the generalization of the case studied previously by Mori and Ando,<sup>40</sup> that describes the coupling between electrons and two-dimensional interface phonons. In this case the interaction matrix element in momentum space reads  $M_q = M_0 e^{-qz}/\sqrt{q}$ , with the distance  $z$  between the electrons and the interface acting as a short-distance cutoff. Performing the Fourier transform we find the Hypergeometric function

$$f(R) = \frac{M_0 \pi^{3/2}}{z^{3/2}} {}_2F_1(3/4, 5/4, 1, -R^2/z^2) \quad (A3)$$

This scales as  $1/R^{3/2}$  for large  $R \gg z$ , and tends to a constant  $f(0) = M_0 \sqrt{\pi}/z^{3/2}$  for  $R \ll z$ . This function is well approximated by the power-law form

$$f(R) = \frac{M'_0}{(R^2 + R_0^2)^{3/4}} \quad (A4)$$



where  $R_0 = (4\sqrt{\pi}c)^{2/3}z \simeq 0.66z$  and  $M'_0 = cM_0$ . It can be easily checked by retransforming back to  $k$ -space that this power-law form gives rise to the correct  $q \rightarrow 0$  limit and lies within 10% of the original one for all  $q \lesssim 1/R_0$ .

Then, in both one and two-dimensional cases, Eqs. (A2,A4) give rise to long range interactions, describing qualitatively similar physical situations. We have chosen to study explicitly the first model in the body of the pa-

per, as in that case the properties of the phononic degrees of freedom can be directly accessed by the solution of a genuinely one dimensional model.

## References

- 
- <sup>1</sup> M. E. Gershenson, V. Podzorov, and A. F. Morpurgo, *Rev. Mod. Phys.* **78**, 973 (2006).
  - <sup>2</sup> T. Holstein, *Ann. of Phys.* **8**, 325 (1959).
  - <sup>3</sup> T. Holstein, *Ann. of Phys.* **8**, 343 (1959).
  - <sup>4</sup> R. Silbey and R. W. Munn, *J. Chem. Phys.* **72**, 2763 (1980).
  - <sup>5</sup> V. M. Kenkre, J. D. Andersen, D. H. Dunlap, and C. B. Duke, *Phys. Rev. Lett.* **62**, 1165 (1989).
  - <sup>6</sup> K. Hannewald *et al.*, *Phys. Rev. B* **69**, 075211 (2004).
  - <sup>7</sup> L. Friedman, *Phys. Rev.* **140**, A1649 (1965).
  - <sup>8</sup> H. Sumi, *J. Chem. Phys.* **70**, 3775 (1979).
  - <sup>9</sup> C. B. Duke and L. B. Schein, *Physics Today* **33**, 42 (1980).
  - <sup>10</sup> A. Troisi and G. Orlandi, *Phys. Rev. Lett.* **96**, 086601 (2006).
  - <sup>11</sup> A. Troisi, *Adv. Mater.* **19**, 2000 (2007).
  - <sup>12</sup> J.-D. Picon, M. N. Bussac, and L. Zuppiroli, *Phys. Rev. B* **75**, 235106 (2007).
  - <sup>13</sup> S. Fratini and S. Ciuchi, *Phys. Rev. Lett.* **103**, 266601 (2009).
  - <sup>14</sup> R. C. Hatch, D. L. Huber, and H. Höchst, *Phys. Rev. Lett.* **104**, 047601 (2010).
  - <sup>15</sup> J. Veres, S. Ogier, S. Leeming, D. Cupertino, and S. M. Khaffaf, *Adv. Funct. Mater.* **13**, 199 (2003).
  - <sup>16</sup> O. D. Jurchescu *et al.*, *Phys. Rev. B* **80**, 085201 (2009).
  - <sup>17</sup> J. Veres, S. Ogier, G. Lloyd, and D. de Leeuw, *Chem. Mater.* **16**, 4543 (2004).
  - <sup>18</sup> T. Richards, M. Bird, and H. Sirringhaus, *J. Chem. Phys.* **128**, 234905 (2008).
  - <sup>19</sup> S. J. Konezny, M. N. Bussac, and L. Zuppiroli, *Phys. Rev. B* **81**, 045313 (2010).
  - <sup>20</sup> T. Cramer *et al.*, *Phys. Rev. B* **79**, 155316 (2009).
  - <sup>21</sup> I. N. Hulea *et al.*, *Nat. Mater.* **5**, 982 (2006).
  - <sup>22</sup> S. Fratini, H. Xie, I. N. Hulea, S. Ciuchi, and A. F. Morpurgo, *New J. Phys.* **10**, 033031 (2008).
  - <sup>23</sup> S. Ciuchi and S. Fratini, *Phys. Rev. B* **79**, 035113 (2009).
  - <sup>24</sup> M. A. Strosio, *Phys. Rev. B* **40**, 6428 (1989).
  - <sup>25</sup> K. W. Kim, M. A. Strosio, A. Bhatt, R. Mickevicius, and V. V. Mitin, *J. Appl. Phys.* **70**, 319 (1991).
  - <sup>26</sup> S. Fratini, A. Morpurgo, and S. Ciuchi, *J. Phys. Chem. Solids* **69**, 2195 (2008).
  - <sup>27</sup> M. Born and R. Oppenheimer, *Ann. der Phys.* **84**, 457 (1927).
  - <sup>28</sup> V. Cataudella, G. De Filippis, and G. Iadonisi, *Phys. Rev. B* **60**, 15163 (1999).
  - <sup>29</sup> V. Cataudella, G. De Filippis, and G. Iadonisi, *Phys. Rev. B* **62**, 1496 (2000).
  - <sup>30</sup> Y. Zhao, D. W. Brown, and K. Lindenberg, *J. Chem. Phys.* **106**, 5622 (1997).
  - <sup>31</sup> D. Feinberg, S. Ciuchi, and F. de Pasquale, *Int. J. of Mod. Phys. B* **4**, 1317 (1990).
  - <sup>32</sup> Y. Toyozawa, *Prog. Theor. Phys.* **26**, 29 (1961).
  - <sup>33</sup> G. De Filippis, to be published.
  - <sup>34</sup> E. Dagotto and A. Moreo, *Phys. Rev. D* **31**, 865 (1985).
  - <sup>35</sup> M. Capone, S. Ciuchi, and C. Grimaldi, *Europhys. Lett.* **42**, 523 (1998).
  - <sup>36</sup> D. Louca, T. Egami, E. L. Brosha, H. Röder, and A. R. Bishop, *Phys. Rev. B* **56**, R8475 (1997).
  - <sup>37</sup> Y. Zhao, G. Li, J. Sun, and W. Wang, *J. Chem. Phys.* **129**, 124114 (2008).
  - <sup>38</sup> A. Alexandrov and P. Kornilovitch, *Phys. Rev. Lett.* **82**, 807 (1999).
  - <sup>39</sup> J. L. H. Fehske and G. Wellein, *Phys. Rev. B* **61**, 8016 (2000).
  - <sup>40</sup> N. Mori and T. Ando, *Phys. Rev. B* **40**, 6175 (1989).
  - <sup>41</sup> M. Capone, W. Stephan, and M. Grilli, *Phys. Rev. B* **56**, 4484 (1997).
  - <sup>42</sup> We note that the site-polaron to bond-polaron transition sharpens upon reducing the LR coupling strength, until it approaches  $\lambda_{SSH} = 0.5$  at  $\lambda_{LR} = 0$ . This value marks the onset of the "pathological" localization found in Ref.[41] in the static phonon limit, where the SSH coupling leads to a two-site polaron dimer that is perfectly isolated from the rest of the system, due to the vanishing of the corresponding transfer integrals. The model remains however well-defined even for larger values  $\lambda_{SSH}$ ,<sup>37</sup> whose analysis is beyond the scope of the present paper.